because of the high incidence of subsequent symptomatic stroke [16]. Therefore, developing novel treatments for carotid artery disease is an urgent task. We have recently established a novel mouse model of bilateral common carotid artery (CCA) gradual occlusion as a mimic of severe carotid artery disease in which multiple cerebral infarctions were induced as a result of cerebrovascular insufficiency [11].

The mouse model is generated by implanting ameroid constrictors (ACs) on the bilateral CCAs, gradually decreasing cerebral blood flow. Multiple cerebral infarctions subsequently develop in the gray and white matter in three-quarters of the animals. As in the case in humans, we hypothesized that cerebral infarctions distal to carotid artery disease could cause neurological and cognitive impairment. To address this question, we studied the behavior of affected mice using a test battery for neurological and cognitive functions. If behavioral phenotypes are recapitulated, this mouse model would further help to investigate the effects of cerebrovascular insufficiency and explore treatments for human carotid artery disease.

2. Materials and methods

2.1. Experimental protocol

Male C57BL/6J mice of 10–12 weeks of age (CLEA Japan, Tokyo) were assigned into the following two groups: (1) sham surgery group ($n = 15$), and (2) AC-implanted group ($n = 29$). Male C57BL/6J male mice aged 1 year old (CLEA Japan, Tokyo) were also used and assigned into the following two groups: (1) sham surgery group ($n = 10$), and (2) AC-implanted group ($n = 10$). After sham surgery or the implantation of AC to each group of mice, neurological and cognitive assessments were made 28 days after surgery in younger mice. Cerebral blood flow (CBF) was assessed by laser speckle flowmetry pre- and post-surgery in both younger and older mice. All mice were housed in a room with a 12-h light/dark cycle (lights on at 7 am) and were given access to food and water ad libitum. We monitored the condition of the animals daily until the 14th day after surgery, after which conditions were monitored twice weekly. All procedures in this study were conducted in strict accordance with the guidelines for animal experimentation from the Animal Research Committee of National Cerebral and Cardiovascular Center. Surgeries were performed under anesthesia, and all efforts were made to minimize suffering.

2.2. Ameroid constrictor (AC)

AC consists of a titanium casing surrounding a hygroscopic casein material with an internal lumen (Tokyo Instruments, Tokyo). The casein component gradually absorbs water and consequently swells, leading to predictable narrowing and occlusion of the arterial lumen it encases. The inner and outer diameters were 0.5 and 3.25 mm, respectively, and the length was 1.28 mm [15].

2.3. Surgical procedure

Under anesthesia with 1.5% isoflurane, the surgery was conducted after confirming the mice were completely static and unresponsive to a toe pinch. Both CCAs were exposed through midline cervical incision and freed from their sheaths. For mice in the AC-implanted group, ACs were applied to the bilateral CCAs. The rectal temperature was maintained between 36.5 °C and 37.5 °C using a self-regulating heating pad.

2.4. Rotarod test

The rotarod test was performed at 28 days after surgery by placing the mouse on a rotating drum (Muromachi Kikai, Tokyo) and measuring the time the mouse maintained its balance on the rod. The speed of the rotarod was accelerated from 4 to 40 rpm over a 5-min period. This test was repeated five times with an interval of 5 min between attempts [20].

2.5. Wire hang test

The wire hang test was performed at 28 days after surgery. A metallic wire (2 mm × 60 cm) was secured to the top of a transparent, rectangular, open-topped plastic box (30 cm height × 60 cm width × 40 cm length). The wire was tightly fixed to the top of the tank to avoid vibration, which could interfere with the performance of mouse. The mice were placed on the metallic wire and latency to fall was recorded. This was repeated five times with an interval of 5 min between attempts. The cutoff time was set at 60 s. Mean latency to fall was determined [20].

2.6. Y-maze test

The Y-maze test was conducted during the dark period (7–11 pm) at 28 days after surgery. This task is based on spontaneous alternation behavior and is used to measure spatial working memory. The maze consists of 3 arms (each 40 cm long, 9.5 cm high, and 4 cm wide), labeled A, B, or C, diverging at 120° angles from a central point. The experiments were performed in a dimly illuminated room. After each mouse was tested, the floor of the maze was cleaned using super hypochlorous water-soaked paper for the discrimination of smell to avoid olfactory cues. Each mouse was placed at the end of the start arm and allowed to move freely through the maze during an 8-min session without reinforcers such as food, water, or electric foot shock. The sequence of arm entries was manually recorded. A mouse was considered to have entered an arm when all 4 paws were positioned in the arm runway. An alternation was defined as entry into all 3 arms on consecutive occasions (e.g., the sequence, ABCBCBCA was counted as 2 alternations, with the first consecutive ABC and the last consecutive BCA out of 6 consecutive occasions; 33% alternations). The maximum alternation was calculated as the total number of arm entries minus 2, and the percentage of alternation was calculated as (actual alternation/maximum alternation) × 100. The total number of arms entered during the sessions, which reflects spontaneous activity, was also recorded. Mice that entered arms less than eight times during the test were eliminated because their data were not considered to reflect precise alternation [21].

2.7. Morris water maze test

The Morris water maze test was performed 28 days after the implantation of AC or sham surgery as previously reported with some modifications [10]. The Morris water maze test consists of a circular pool (diameter, 120 cm; depth, 40 cm) and a set of video analysis systems (EthoVision XT5; Noldus, Wageningen, Netherlands). The pool was filled with water containing non-toxic white paint to a depth of 30 cm. A clear, circular platform (diameter, 8 cm) was submerged 1 cm below the water surface in the center of one quadrant of the pool (target quadrant). Red cross sign and blue upward arrow at the opposite side of red cross sign were used as the cues for the mice to orient for swimming in the pool. On the first 4 days, we performed four trials per day with a 5-min interval between attempts (acquisition phase). The platform was kept in the same position during the acquisition phase. The mice were placed at the starting position (the quadrant adjacent to the

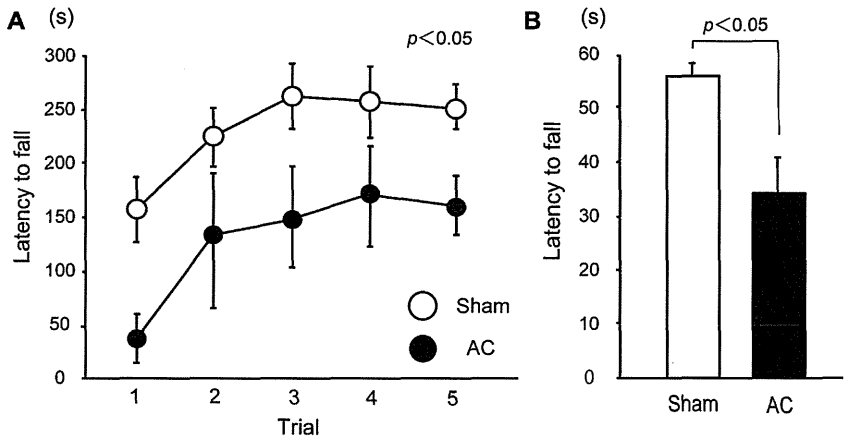

Fig. 1. Motor deficits of ameroid constrictor (AC)-implanted mice. Histograms show latency to fall of sham surgery ($n = 15$) and AC-implanted mice ($n = 7$) in the rotarod test (A) and wire hang test (B). Data were analyzed by two-way repeated-measures ANOVA (A) and unpaired t-test (B).

target one; cf. Zone 2 at Fig. 3C) and released into the water. Each mouse was allowed to swim for 60 s, discover the hidden platform, and climb onto it. The trial was immediately terminated after the mouse arrived on the platform or after 60 s had elapsed. When a mouse succeeded in climbing onto the platform, it was permitted to remain there for 10 s. If a mouse did not reach the platform within 60 s, it was placed there and allowed to remain for 15 s. Latency to reach the platform (escape latency) and mean swimming speed were recorded. On the 5th day (the last day), the mice were subjected to the probe trial session in which the platform was removed from the pool and the mice were allowed to swim for 60 s to search for it. The duration of swimming in each quadrant was recorded.

2.8. Measurement of CBF by laser speckle flowmetry

Relative CBF was determined by laser speckle flowmetry (Onegazone; Omegawave, Tokyo), which obtains high resolution, two-dimensional imaging and has a linear relationship with absolute CBF values [1]. Recordings were performed through the skull under 1.5% isoflurane anesthesia. The periosteum, which adheres to the skull, was widely removed with fine-tip forceps. For each recording, the skull surface was wiped with saline-soaked gauze and then covered with a thin layer of gel to prevent drying.

2.9. Statistical analysis

All values are expressed as mean ± standard error in the text and figures. Differences with $p < 0.05$ were considered statistically significant in all analyses, which included the Student's t-test and two-way repeated-measures analysis of variance (ANOVA).

3. Results

Several behavioral tests were assessed in seven AC-implanted mice that survived for 28 days following surgery and compared with those of 15 sham-surgery mice. We investigated motor coordination and balance using the rotarod test, muscle strength using the wire hang test, and learning and memory using the Y-maze and Morris water maze tests.

In the rotarod test, latency to fall was significantly shorter in AC-implanted mice than in sham surgery mice, suggesting that AC-implanted mice had motor incoordination and imbalance (Fig. 1A). In the wire hang test, results showed that latency to fall was significantly shorter in AC-implanted mice than in the sham surgery mice, indicating that AC-implanted mice suffered from neuromuscular weakness (Fig. 1B). In the Y-maze test, the percentage of alternation behaviors significantly decreased in AC-implanted mice compared with that in the sham surgery mice (Fig. 2A). This result indicates that AC-implanted mice developed working memory impairment.

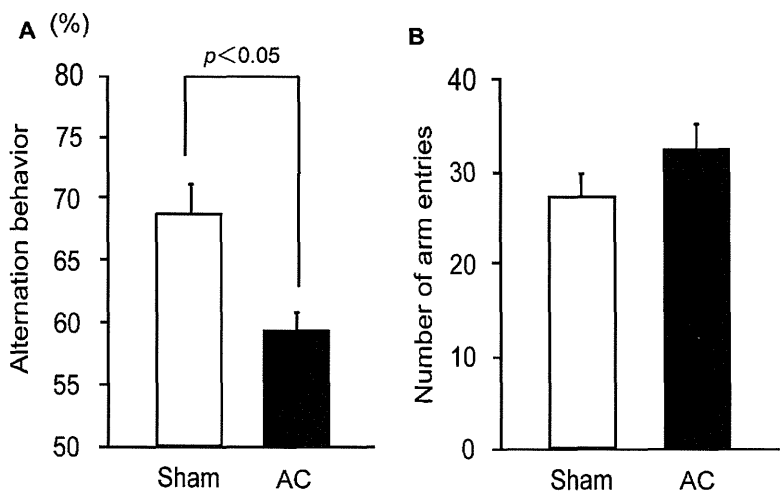

Fig. 2. Working memory impairment of AC-implanted mice. Histograms show percentage of spontaneous alteration behavior (A) and number of arm entries (B) of sham surgery mice ($n = 15$) and AC-implanted mice ($n = 7$) in the Y-maze test. Data were analyzed by unpaired t-test.

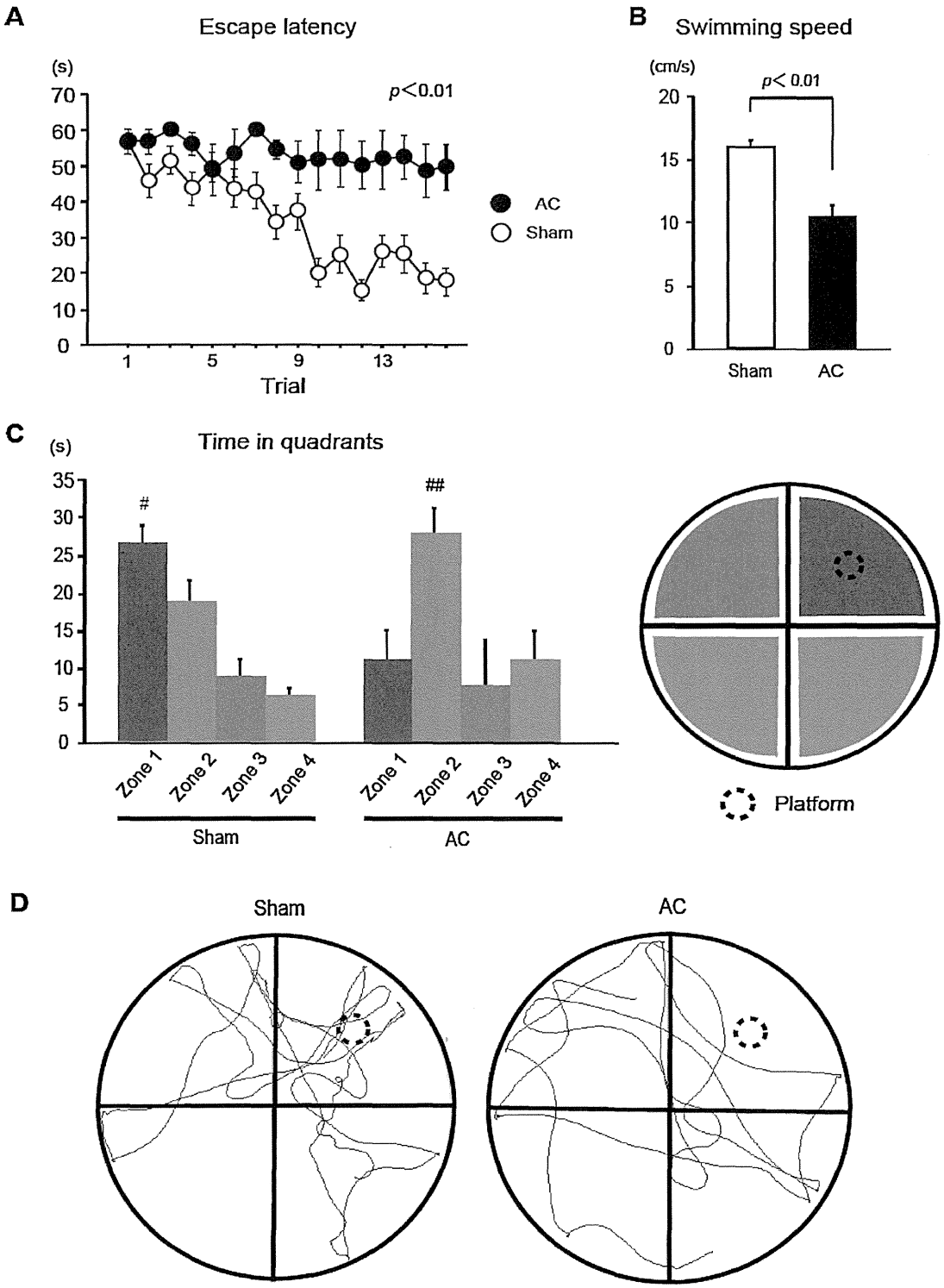

Fig. 3. Spatial learning and reference memory impairment of AC-implanted mice. Escape latency in acquisition phase (A), swimming speed in acquisition phase (B), time staying in each quadrant in probe trial (C), and representative swimming traces of the swim pattern in probe trial (D) of sham surgery mice ($n = 15$) and AC-implanted mice ($n = 7$) in the Morris water maze test. Data were analyzed by two-way repeated-measures ANOVA (A) and unpaired t-test (B and C). $^{\#}p < 0.05$ vs. Zones 2–4; $^{\#\#}p < 0.01$ vs. Zones 1, 3, and 4.

However, the number of arm entries did not differ between the two groups, reflecting that the extent of spontaneous activity was similar between the groups (Fig. 2B). Finally we performed the Morris water maze test. In the acquisition phase, AC-implanted mice showed significantly longer escape latency compared with the sham surgery mice (Fig. 3A). Swimming speed was significantly slower in AC-implanted mice (Fig. 3B). In the probe trial, AC-implanted mice did not stay longer in Zone 1 (target quadrant) than other quadrants, whereas the sham surgery mice stayed for the longest time in Zone 1, indicating that the sham surgery mice remembered where the platform had been (Fig. 3C and D). These results show that AC-implanted mice developed spatial learning and reference memory impairment together with motor impairment and loss of motivation.

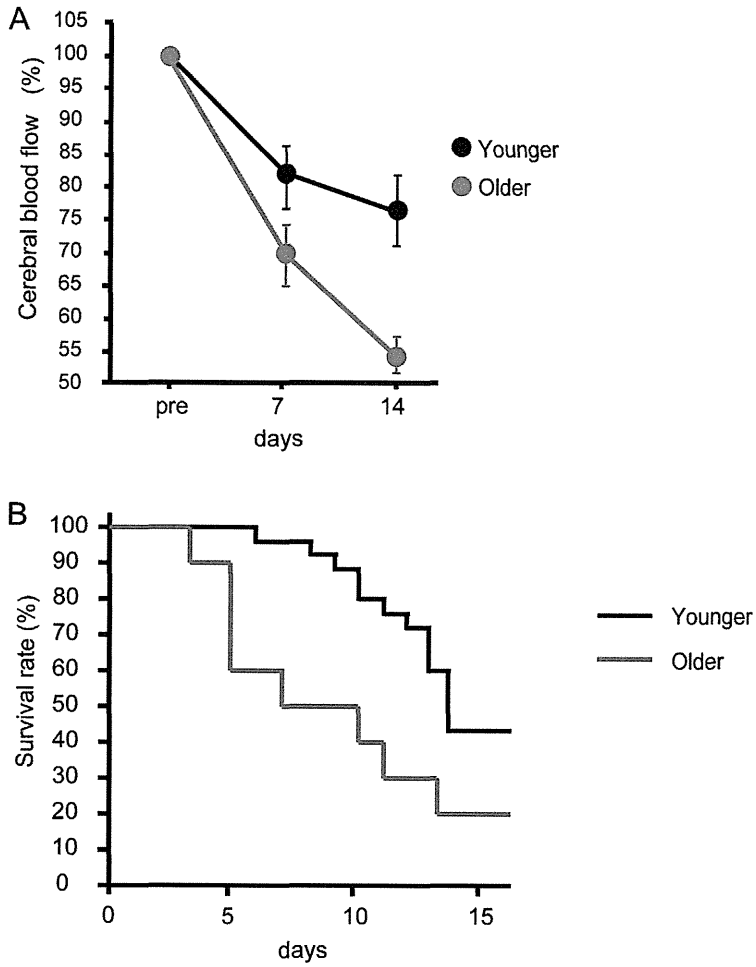

Fig. 4. Temporal profile of CBF and survival rate of AC-implanted older mice. (A) The degree of CBF reduction after AC-implantation tends to be substantially different between the surviving older ($n=2$) and younger ($n=8$) mice at 7 and 14 days post-surgery. (B) The Kaplan–Meier curves show a significantly lower survival rate in the older mice compared to the younger mice after implantation of ACs (younger mice, $n=29$; older mice, $n=10$).

We also conducted the same surgery to the older mice. The laser speckle flowmetry showed that CBF of AC-implanted older mice gradually decreased up to approximately 53.7% of baseline level that tended to be lower than the AC-implanted younger mice (Fig. 4A). The survival rate was significantly lower; 8 of 10 (80%) of the AC-implanted older mice died by day 15 post-surgery (Fig. 4B).

4. Discussion

These studies of our recently established mouse model of carotid artery disease [11] show that affected mice experience (1) motor incoordination and imbalance, (2) neuromuscular weakness, (3) working memory impairment, and (4) spatial learning and reference memory impairment.

Carotid atherosclerosis is one of the most significant risk factors for transient ischemic attack (TIA) and symptomatic cerebral infarctions. The mechanism may be embolism of thrombotic material or low perfusion because of stenosis with inadequate collateral compensation [7,8,14,17]. The rate of symptoms caused by cerebral ischemia increases in parallel with the severity of carotid artery stenosis/occlusion [4]. Bilateral internal carotid artery occlusion causes TIA in 21–73% of patients and symptomatic ischemic stroke in 63–66%, whereas bilateral CCA occlusion causes TIA in 72% and symptomatic ischemic stroke in 71% [16,19]. This study shows that our model replicates disabling motor activity caused by cerebral infarction, reflecting the condition of patients with severe carotid artery disease.

High-grade carotid artery stenosis causes cognitive impairment and decline because of hemodynamic impairment [2], even in patients without clinically evident cerebrovascular disease [13]. Scores on mini-mental state examinations decrease over 3–5 years in patients with severe carotid artery disease [2,13]. The results of the Y-maze test indicate that bilateral CCA gradual occlusion causes impaired working memory, which is consistent with the finding that the model mice develop frontal white matter lesions [11]. As shown previously, working memory can be impaired by damage to the fronto-subcortical circuits in rodents [20]. In addition, the results of the Morris water maze test indicate that bilateral CCA gradual occlusion leads to impairment of spatial learning and reference memory, solely relying on the function of the hippocampus [3], which is consistent with the finding that most of the model mice develop hippocampal neuronal loss [11]. Therefore, this study shows that bilateral CCA gradual occlusion in this mouse model leads to both hippocampus-dependent and -independent memory impairment because of cerebral infarctions induced by cerebrovascular insufficiency, replicating the cognitive status of patients with severe carotid artery disease.

Given the fact that the brains of older mice, like humans, react differently to ischemic insults compared to younger mice, we assessed CBF and survival rate of AC-implanted one-year-old mice. Probably due to vulnerability to ischemic insult, the older mice died

earlier than the younger mice, which made modeling difficult using ACs in aged mice. Because aging processes include rarefaction of the native leptomeningeal collateral vasculature [6], CCA gradual occlusion may have led to a more severe ischemic tissue injury in C57BL/6J mice.

5. Conclusion

We successfully developed a novel mouse model of ischemic carotid artery disease that shows neurological deficits and cognitive abnormalities with severe cerebrovascular insufficiency. The current model will be useful for investigating the mechanisms underlying neurological and cognitive deficits following cerebrovascular insufficiency and exploring pharmacological interventions in stroke patients with severe carotid artery disease.

Acknowledgment

We gratefully acknowledge grant support from the Ministry of Health, Labour and Welfare (M.I., No. 0605-1).

References

[1] C. Ayata, A.K. Dunn, Y. Gursoy-OZdemir, Z. Huang, D.A. Boas, M.A. Moskowitz, Laser speckle flowmetry for the study of cerebrovascular physiology in normal and ischemic mouse cortex, J. Cereb. Blood Flow Metab. 24 (2004) 744–755.
[2] S. Balestrini, C. Perozzi, C. Altamura, F. Vernieri, S. Luzzi, M. Bartolini, L. Provinciali, M. Silvestrini, Severe carotid stenosis and impaired cerebral hemodynamics can influence cognitive deterioration, Neurology 80 (2013) 2145–2150.
[3] F. Block, M. Schwarz, Correlation between hippocampal neuronal damage and spatial learning deficit due to global ischemia, Pharmacol. Biochem. Behav. 56 (1997) 755–761.
[4] Q. Chen, Y. Liu, L. Pei, D. Ke, G. Li, W. Deng, W. Yao, Characteristics of carotid artery disease (CAD) and presenting cerebrovascular symptoms in an aged group, Int. J. Cardiovasc. Imaging 25 (2009) 127–132.
[5] D.W. Droste, C. Iliescu, M. Vaillant, N. De Bremaeker, C. Lieunard, M. Meyer, A. Kuemmerie, A. Chioti, Lifestyle counseling in patients with carotid arteriosclerosis from Luxemburg should focus more on the reduction of sugar, sodium and saturated fat consumption, Bull. Soc. Sci. Med. Grand Duche. Luxemb. 1 (2013) 28–38.
[6] J.E. Faber, H. Zhang, R.M. Lassance-Soares, P. Prabhakar, A.H. Najafi, M.S. Burnett, S.E. Epstein, Aging causes collateral rarefaction and increased severity of ischemic injury in multiple tissues, Arterioscler. Thromb. Vasc. Biol. 31 (2011) 1748–1756.
[7] C.M. Fisher, Concerning recurrent transient cerebral ischemic attacks, Can. Med. Assoc. J. 86 (1962) 1091–1099.
[8] M. Fisher, Occlusion of the internal carotid artery, A.M.A. Arch. Neurol. Psychiatry 65 (1951) 346–377.
[9] E.S. Ford, W.H. Giles, A.H. Mokdad, Increasing prevalence of the metabolic syndrome among U.S. Adults, Diabetes Care 27 (2004) 2444–2449.
[10] G.A. Fridgeirsdottir, L. Hillfred, Escalated handling of young C57BL/6 mice results in altered Morris water maze performance, Upsala J. Med. Sci. 119 (2014) 1–9.
[11] Y. Hattori, A. Kitamura, K. Nagatsuka, M. Ihara, A novel mouse model of ischemic carotid artery disease, PLOS ONE 9 (2014) e100257.
[12] M. Herder, K.A. Arntzen, S.H. Johnsen, E.B. Mathiesen, The metabolic syndrome and progression of carotid atherosclerosis over 13 years. The Tromsø study, Cardiovasc. Diabetol. 11 (2012) 77.
[13] S.C. Johnston, E.S. O'Meara, T.A. Manolio, D. Lefkowitz, D.H. O'Leary, S. Goldstein, M.C. Carlson, L.P. Fried, W.T. Longstreth Jr., Cognitive impairment and decline are associated with carotid artery disease in patients without clinically evident cerebrovascular disease, Ann. Intern. Med. 140 (2004) 237–247.
[14] J.P. Kistler, A.H. Ropper, R.C. Heros, Therapy of ischemic cerebral vascular disease due to atherothrombosis (1), N. Eng. J. Med. 311 (1984) 27–34.
[15] A. Kitamura, Y. Fujita, N. Oishi, R.N. Kalaria, K. Washida, T. Maki, Y. Okamoto, Y. Hase, M. Yamada, J. Takahashi, H. Ito, H. Tomimoto, H. Fukuyama, R. Takahashi, M. Ihara, Selective white matter abnormalities in a novel rat model of vascular dementia, Neurobiol. Aging 33 (2012), pp. 1012 e1025–1012 e1035.
[16] S.L. Lai, Y.C. Chen, H.H. Weng, S.T. Chen, S.P. Hsu, T.H. Lee, Bilateral common carotid artery occlusion – a case report and literature review, J. Neurol. Sci. 238 (2005) 101–104.
[17] J.P. Mohr, Transient ischemic attacks and the prevention of strokes, N. Eng. J. Med. 299 (1978) 93–95.
[18] R.R. Moustafa, D. Izquierdo-Garcia, P.S. Jones, M.J. Graves, T.D. Fryer, J.H. Gillard, E.A. Warburton, J.C. Baron, Watershed infarcts in transient ischemic attack/minor stroke with ≥50% carotid stenosis: hemodynamic or embolic? Stroke 41 (2010) 1410–1416.
[19] S. Persoon, C.J. Klijn, A. Algra, L.J. Kappelle, Bilateral carotid artery occlusion with transient or moderately disabling ischaemic stroke: clinical features and long-term outcome, J. Neurol. 256 (2009) 1728–1735.
[20] M. Shibata, N. Yamasaki, T. Miyakawa, R.N. Kalaria, Y. Fujita, R. Ohtani, M. Ihara, R. Takahashi, H. Tomimoto, Selective impairment of working memory in a mouse model of chronic cerebral hypoperfusion, Stroke 38 (2007) 2826–2832.
[21] K. Washida, M. Ihara, K. Nishio, Y. Fujita, T. Maki, M. Yamada, J. Takahashi, X. Wu, T. Kihara, H. Ito, H. Tomimoto, R. Takahashi, Nonhypotensive dose of telmisartan attenuates cognitive impairment partially due to peroxisome proliferator-activated receptor-gamma activation in mice with chronic cerebral hypoperfusion, Stroke 41 (2010) 1798–1806.

ANNALS of Clinical and Translational Neurology
Open Access

RESEARCH ARTICLE

Phosphodiesterase III inhibitor promotes drainage of cerebrovascular β-amyloid

Takakuni Maki[1,2], Yoko Okamoto[1,3], Roxana O. Carare[4], Yoshiki Hase[1], Yorito Hattori[1,5], Cheryl A. Hawkes[4], Satoshi Saito[1,5], Yumi Yamamoto[5], Yasukazu Terasaki[2], Hatsue Ishibashi-Ueda[3], Akihiko Taguchi[6], Ryosuke Takahashi[1], Taihei Miyakawa[7], Raj N. Kalaria[8], Eng H. Lo[2], Ken Arai[2] & Masafumi Ihara[1,9]

[1]Department of Neurology, Graduate School of Medicine, Kyoto University, Kyoto, Japan
[2]Departments of Radiology and Neurology, Massachusetts General Hospital and Harvard Medical School, Charlestown, Massachusetts
[3]Department of Pathology, National Cerebral and Cardiovascular Center, Osaka, Japan
[4]Division of Clinical Neurosciences, Southampton General Hospital, Southampton University, Hampshire, United Kingdom
[5]Department of Regenerative Medicine and Tissue Engineering, National Cerebral and Cardiovascular Center, Osaka, Japan
[6]Department of Regenerative Medicine Research, Institute of Biomedical Research and Innovation, Kobe, Japan
[7]Amakusa Hospital, Kumamoto, Japan
[8]Institute for Ageing and Health, NIHR Biomedical Research Building, Newcastle University, Campus for Ageing and Vitality, Newcastle upon Tyne, United Kingdom
[9]Department of Stroke and Cerebrovascular Diseases, National Cerebral and Cardiovascular Center, Osaka, Japan

Correspondence
Masafumi Ihara, Department of Stroke and Cerebrovascular Diseases, National Cerebral and Cardiovascular Center, 5-7-1 Fujishiro-dai, Suita, Osaka 565-8565, Japan. Tel: +81-6-6833-5012; Fax: +81-6-6835-5137; E-mail:ihara@ncvc.go.jp
Takakuni Maki, Departments of Radiology and Neurology, Massachusetts General Hospital and Harvard Medical School, MGH East 149-2401, Charlestown, MA 02129. Tel: +1-617-724-9503; Fax: +1-612-726-7830; E-mail: tmaki@partners.org

Funding Information
We gratefully acknowledge grant support from the Ministry of Health, Labour and Welfare (M. I., No. 0605-1), the Ministry of Education, Culture, Sports, Science and Technology (M. I., Scientific Research (B), No. 23390233), the Takeda Science Foundation (M. I.), the National Institutes of Health (K. A., E. H. L., P01 NS055104; K. A., R01 NS065089; E. H. L., R37 NS037074), the Research Councils UK and Alzheimer's Research UK (R. N. K.), the Japan Society for the Promotion of Science (T. M.), and the Uehara Memorial Foundation (T. M.).

Received: 17 December 2013; Revised: 9 April 2014; Accepted: 2 June 2014

Annals of Clinical and Translational Neurology **2014; 1(8): 519–533**

doi: 10.1002/acn3.79

Abstract

Objective: Brain amyloidosis is a key feature of Alzheimer's disease (AD). It also incorporates cerebrovascular amyloid β (Aβ) in the form of cerebral amyloid angiopathy (CAA) involving neurovascular dysfunction. We have recently shown by retrospective analysis that patients with mild cognitive impairment receiving a vasoactive drug cilostazol, a selective inhibitor of phosphodiesterase (PDE) III, exhibit significantly reduced cognitive decline. Here, we tested whether cilostazol protects against the disruption of the neurovascular unit and facilitates the arterial pulsation-driven perivascular drainage of Aβ in AD/CAA. **Methods:** We explored the expression of PDE III in postmortem human brain tissue followed by a series of experiments examining the effects of cilostazol on Aβ metabolism in transgenic mice (Tg-SwDI mice) as a model of cerebrovascular β-amyloidosis, as well as cultured neurons. **Results:** We established that PDE III is abnormally upregulated in cerebral blood vessels of AD and CAA subjects and closely correlates with vascular amyloid burden. Furthermore, we demonstrated that cilostazol treatment maintained cerebral hyperemic and vasodilative responses to hypercapnia and acetylcholine, suppressed degeneration of pericytes and vascular smooth muscle cells, promoted perivascular drainage of soluble fluorescent $A\beta_{1\text{-}40}$, and rescued cognitive deficits in Tg-SwDI mice. Although cilostazol decreased endogenous Aβ production in cultured neurons, C-terminal fragment of amyloid precursor protein expression was not altered in cilostazol-treated Tg-SwDI mice. **Interpretation:** The predominant action of cilostazol on Aβ metabolism is likely to facilitate Aβ clearance due to the sustained cerebrovascular function in vivo. Our findings mechanistically demonstrate that cilostazol is a promising therapeutic approach for AD and CAA.

Introduction

Alzheimer's disease (AD) is the most common form of dementia. In addition to neurofibrillary tangles (NFTs), the major pathological features in AD comprise brain accumulation of amyloid β peptide (Aβ) as senile plaques and in the form of cerebral amyloid angiopathy (CAA).[1] The deposition of Aβ in cerebral blood vessels influences vascular function and worsens the pathology contributing to cognitive decline.[2–6] Recent studies suggest reduced Aβ clearance from the brain rather than increased Aβ production is responsible for Aβ accumulation in the brain in the common late-onset form of AD.[7] Aβ may be degraded by glial cells,[8,9] and proteases (e.g., by neprilysin or insulin degrading enzyme)[10] and is transported across the endothelium by the low-density lipoprotein receptor-related protein 1 (LRP-1) or the receptor for advanced glycation end products (RAGE).[11,12] The drainage of extracellular Aβ along the basement membranes of capillaries and arteries appears as the most important mechanism for removal of Aβ from the brain.[3,13,14] Besides impacting on the structural and functional components of the neurovascular unit, deposition of Aβ within the perivascular drainage pathway lowers the motive force of Aβ clearance, thereby contributing to increased parenchymal Aβ deposition.[15,16] Indeed, a recent study using real-time imaging showed direct evidence that tracers injected into the living mouse brain were cleared along arteries and capillaries but not veins.[17] Solute clearance along the perivascular route was impaired in mice with hemodynamic insufficiency as well as in APPswe/PS1dE9 transgenic mice, which develop parenchymal and microvascular amyloid deposits.[17] Consistent with such findings, immunotherapy intended to reverse the accumulation of Aβ plaques in the brain has been shown to concomitantly increase cerebrovascular Aβ and exacerbate microvascular lesions.[18,19] Unusually high levels of soluble Aβ have been also detected in the brains of immunized AD patients.[20] These results suggest that Aβ immunization may result in the failure of efficient perivascular drainage of Aβ solubilized from plaques resulting in an increase in the severity of CAA.[18,21] Thus, approaches that enhance Aβ clearance via perivascular drainage and protect the neurovascular unit hold promise for the development of novel therapies for AD.

Cyclic nucleotide phosphodiesterases (PDEs) play critical roles in regulating intracellular cyclic nucleotides (cyclic adenosine monophosphate (cAMP) and cyclic guanosine monophosphate), which are important second messengers involved in intracellular signal transduction in all tissues. Thus far, 11 PDE families have been described, most of them are expressed in the brain, attracting attention as a source of new targets for the treatment of psychiatric and neurodegenerative disorders.[22,23] PDE III, PDE IV, or PDE V inhibitors have been shown to have positive effects on the pathology and behavior in several animal models of AD[22–25] and human studies of AD patients.[26,27] Most of these studies were based on the perspective of neuronal/synaptic and glial dysfunction, and impairment of neurogenesis and synaptic resilience in AD models and patients. However, considering that vascular impairment in the context of neurovascular unit is also closely associated with the pathogenesis of AD/CAA[28,29] and the failure of Aβ immunotherapy,[18,20] restoring vascular integrity in addition to neuronal/synaptic and glial function should be crucial for the treatment of AD/CAA.

PDE III is the major cAMP-hydrolyzing PDE (a negative regulator of cAMP) uniquely expressed in vascular smooth muscle cells, and PDE IIIA isoforms are also involved in cardiovascular function by regulating vascular smooth muscle growth regulation and phenotypic changes. Cilostazol, a selective inhibitor of PDE III, increases cAMP in vascular cells and has multiple effects on the vasculature such as vasodilatation, anti-oxidation, anti-inflammation, regulation of smooth muscle cell,[30] increase in cerebral hemodynamics,[31] pulse duration time[32] and arterial elasticity[33] with maintenance of microvascular integrity.[34] We have recently shown that patients with mild cognitive impairment receiving cilostazol exhibit significantly reduced cognitive decline,[35,36] suggesting that cilostazol, originally a drug for stroke and peripheral arterial disease, is effective for dementing disorders through its action on the vasculature and providing rationale of experimental study using an animal model of cerebrovascular β-amyloidosis.

Given the rationale and background outlined above, we first explored the expression of PDE III in postmortem human brains followed by a series of experiments using transgenic mice (Tg-SwDI mice) expressing the Swedish (K670/M671L) and vasculotropic Dutch/Iowa (E693Q/D694N) mutant of the human amyloid precursor protein (APP) to examine whether cilostazol protected against the disruption of the neurovascular unit and rescued the perivascular drainage of Aβ in AD/CAA. We further investigated whether cilostazol is beneficial or improves vascular reactivity, cerebral blood flow (CBF), perivascular Aβ drainage, vascular morphology, and behavioral/cognitive function in the transgenic mice, which exhibit deficient cerebral clearance of Aβ.[37] Furthermore, we examined whether cilostazol can alter the Aβ biogenesis in cultured neurons as well as the in vivo

system. These experimental approaches provide strong rationale for placebo-controlled pharmacological trials to establish the efficacy of cilostazol in patients with AD/CAA.

Subjects/Materials and Methods

Postmortem human brain material

Autopsied brains were obtained from Kyoto University Hospital through a process approved by an institutional research committee. Methods and relevant references are available in the Data S1.

Experimental study

We used transgenic mice, C57BL/6-Tg(Thy1-APPSwDutIowa) BWevn/J (Jackson Laboratory, Bar Harbor, ME) as a CAA mouse model. Experimental details are available in the Data S1.

Results

PDE III, a negative regulator of cAMP, was abnormally expressed in the cerebral vessels of AD/CAA patients and correlated with the vascular amyloid burden

On the basis that PDE III is a vasoactive enzyme uniquely expressed in vascular smooth muscle cells and plays a pivotal role in vascular function, we evaluated PDE IIIA immunoreactivity in postmortem human brains. The demographic details and pathological findings are summarized in Table S1. PDE IIIA immunostaining was negligible in the brain without CAA (Fig. 1A–C). In contrast, PDE IIIA-immunoreactivity was upregulated mostly in the vascular smooth muscle cells, of both the leptomeningeal and cortical arteries as CAA severity increased (Fig. 1D–L and N) with a significant linear correlation ($Rs = 0.8272$, $P < 0.001$ for Spearman's rank correlation

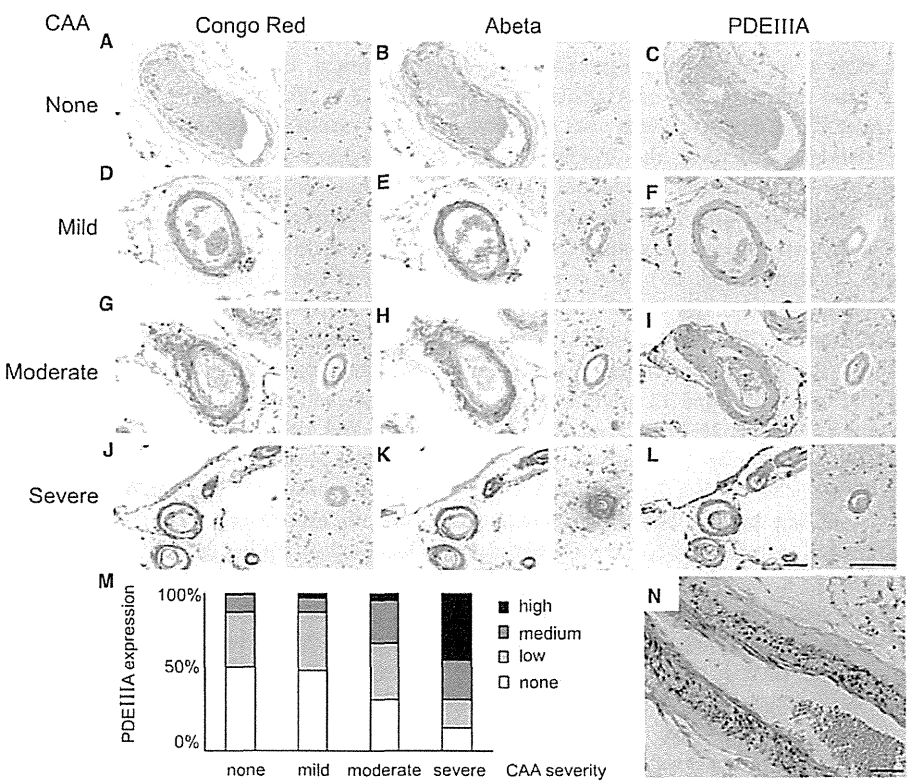

Figure 1. PDE IIIA expression is upregulated in the vascular wall in close correlation with CAA severity. (A–L and N) Representative images of Congo red staining (A, D, G and J), Aβ immunostaining (B, E, H and K), and PDE IIIA immunostaining (C, F, I, L and N) in the leptomeningeal (left) and intracerebral cortical (right) vessels of patients without CAA (A–C) and with mild CAA (D–F), moderate CAA (G–I), and severe CAA (J–L and N). Scale bar indicates 100 μm. (M) Histogram showing the percentage of vessels with PDE IIIA expression (none, low, medium, and high) in patients without CAA and with mild, moderate, and severe CAA. PDE, phosphodiesterases; CAA, cerebral amyloid angiopathy.

coefficient, Fig. S1). Two relatively pure CAA cases (Case No. 9 and 15; moderate and severe, respectively) showed increased PDEIII expression, while two controls (Case No. 16 and 17) without brain pathology showed lower PDEIII expression score (Table S1). PDE IIIA was also detected in the parenchyma (Fig. S2A–C). Some of the cortical capillaries exhibited PDE IIIA immunostaining in the vascular walls suggestive of pericytes (Fig. S2D and E). Some of neurons including dystrophic neurites around the amyloid core showed PDE IIIA expression (Fig. S3E–L). However, neuropil threads and amyloid cores did not express PDE IIIA (Fig. S3E–L). The aged Tg-SwDI mice also showed the increased expression of PDE IIIA in the vascular wall of the leptomeningeal and intracortical arteries (Fig. S4). These results suggested that PDE IIIA expression is abnormally upregulated especially in the vascular smooth muscle cells in close correlation with the vascular amyloid burden.

Cilostazol restored vasoreactivity in Tg-SwDI mice

Impairments in cerebral circulation and vascular reactivity have substantial roles in the onset and progression of AD/CAA in human[38] and mouse models of AD/CAA including Tg-SwDI mice.[5,39] Consistent with the previous reports, which demonstrated that the Tg-SwDI mice showed microvascular Aβ deposition throughout the forebrain by 12 months of age,[37] most of the vessels were affected by microvascular amyloid in vehicle-treated Tg-SwDI mice aged 23 months (Fig. S5). We first investigated whether cilostazol ameliorates vascular dysfunction in Tg-SwDI mice. Resting CBF was marginally increased in cilostazol-treated Tg-SwDI mice compared with vehicle-treated Tg-SwDI mice both aged 12 months (8-month cilostazol treatment vs. vehicle; 26.7 ± 1.3 vs. 25.1 ± 1.1, $P = 0.13$) and aged 15 months (13.5-month cilostazol treatment on vs. vehicle; 27.9 ± 2.9 vs. 26.1 ± 3.2, $P = 0.09$) (Fig. 2A–D; left panels) but these increments did not reach statistical significance. However, cilostazol-treated mice showed a significant increase in CBF response to hypercapnia compared with vehicle-treated Tg-SwDI mice both aged 12 months (8-month cilostazol treatment vs. vehicle; 28.0 ± 4.3% vs. 19.6 ± 2.2%; $P = 0.0495$) and aged 15 months (13.5-month cilostazol treatment vs. vehicle; 24.3 ± 6.1% vs. 15.5 ± 3.9%, $P < 0.01$) (Fig. 2A–D; right panels). We evaluated the vasodilatory response to hypercapnia and acetylcholine using in vivo imaging (Fig. S6). We assessed the vessels that are comparable in the baseline vascular diameters between the treated and untreated groups (Fig. 2E and F; left panels). However, cilostazol-treated Tg-SwDI mice showed significant increases in the vasodilatory response to hypercapnia (Fig. 2E and F; right panels) and acetylcholine both aged 12 months (8-month cilostazol treatment vs. vehicle; 19.0 ± 3.2% vs. 12.1 ± 2.9% for hypercapnia, $P = 0.0495$; 17.4 ± 2.3% vs. 11.2 ± 3.6%, $P = 0.0495$ for acetylcholine) (Fig. 2G) and aged 15 months (13.5-month cilostazol treatment vs. vehicle; 16.3 ± 4.5% vs. 11.5 ± 1.1% for hypercapnia, $P < 0.01$; 14.7 ± 3.2% vs. 9.3 ± 0.8% for acetylcholine, $P = 0.032$) (Fig. 2H). This was consistent with the results of CBF response. These findings indicated that cilostazol restores cerebral hemodynamic reserve in Tg-SwDI mice.

Cilostazol facilitated perivascular drainage of Aβ in Tg-SwDI mice

Cerebrovascular dysfunction and reduced arterial pulsations may result in the failure of perivascular drainage of soluble Aβ, leading to the accumulation and aggregation of Aβ in the vessel walls and in the brain parenchyma.[17] We investigated whether the restoration of vascular reactivity by cilostazol led to an improvement of perivascular drainage of soluble Aβ in Tg-SwDI mice. Intracerebral injections of soluble fluorescent HiLyte Aβ tracers were performed, following the methodology described before[13] (Fig. 3A). Thirty minutes after the injection into the striatum, soluble fluorescent $Aβ_{1-40}$ had spread diffusely throughout the brain parenchyma and was present within the basement membranes of parenchymal and leptomeningeal arteries. At 30 min post-injection, most of the Aβ had drained out of the brain from the site of injection and Aβ was detected only in the leptomeningeal arteries (Fig. 3B), and within Iba-1-positive microglia as well as NeuN-positive neurons (data not shown). Within the leptomeningeal arteries, Aβ was located outside the platelet endothelial cell adhesion molecule-1-positive endothelial cells and colocalized with smooth muscle actin-positive vascular smooth muscle cells (data not shown) and the laminin present in the basement membranes surrounding smooth muscle cells (Fig. 3C). The radial spread of Aβ localized in the leptomeningeal arteries from the injection site was calculated. We did not quantify the fluorescent Aβ -positive vessels around the needle tract as they could be technical artifacts. The number of vessels analyzed was similar for vehicle- and cilostazol-treated Tg-SwDI mice (cilostazol vs. vehicle; 31 ± 3.7 vs. 29 ± 7.0). There were marginally significant and significant differences in the averaged and maximal radial spread of fluorescent $Aβ_{1-40}$, respectively, between vehicle- and cilostazol-treated Tg-SwDI mice at 15 months of age (13.5-month cilostazol treatment vs. vehicle; 2783 ± 234 μm vs. 2395 ± 186 μm for average spread, $P = 0.057$; 3678 ± 238 μm vs. 2820 ± 386 μm for maximum spread, $P = 0.028$) (Fig. 3D and E). These results suggest that long-term

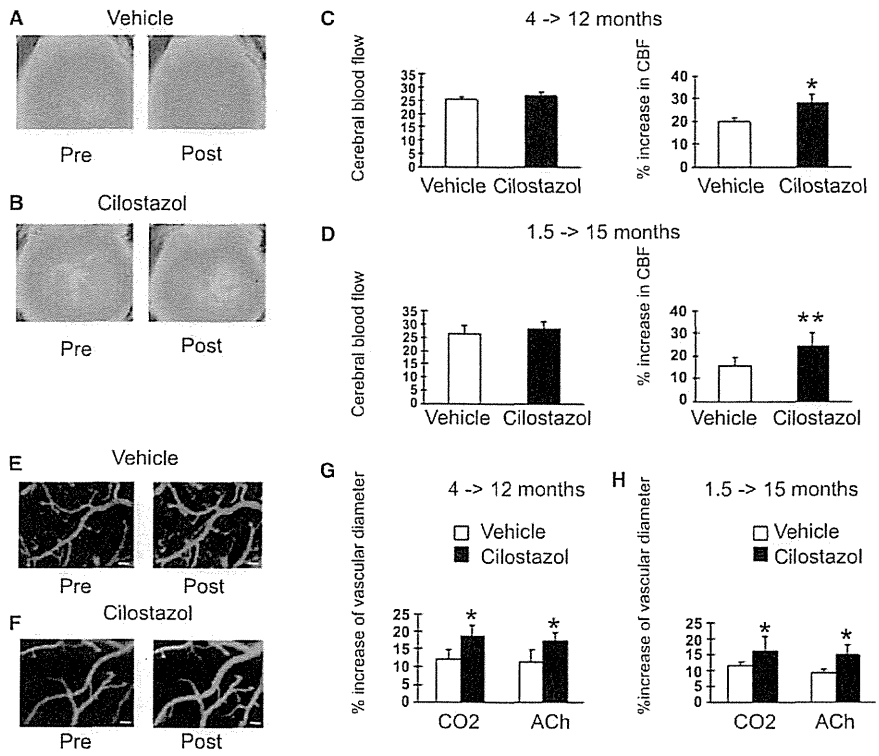

Figure 2. Cilostazol-treated Tg-SwDI mice exhibit increased cerebral blood flow response to hypercapnia and increased vasodilative response to hyperacapnia and acetylcholine. (A and B) Representative images showing temporal changes of cerebral blood flow (CBF) before (Pre) and after (Post) hypercapnia in vehicle-treated and cilostazol-treated Tg-SwDI mice. (C) Histogram showing CBF (left) and % increase in CBF (right) in vehicle-treated (n = 3) and cilostazol-treated (n = 3) Tg-SwDI mice aged 12 months treated from aged 4 months. (D) Histogram showing CBF (left) and % increase in CBF (right) in vehicle-treated (n = 7) and cilostazol-treated (n = 9) Tg-SwDI mice aged 15 months treated from aged 1.5 months. Error bars indicate SD. $^{**}P < 0.01$ and $^{*}P < 0.05$ in vehicle-treated Tg-SwDI mice versus cilostazol-treated Tg-SwDI mice. (E and F) Representative images showing temporal changes of leptomeningeal arteries before (left) and after (right) hypercapnia in vehicle-treated (E) and cilostazol-treated (F) mice. Scale bars indicate 50 μm. (G) Histogram showing % increase of vascular diameter in response to hypercapnia (left) and acetylcholine (ACh, right) in vehicle-treated (n = 3) and cilostazol-treated (n = 3) Tg-SwDI mice aged 12 months treated from aged 4 months. (H) Histograms showing % increase of vascular diameter in response to hypercapnia (left) and acetylcholine (right) in vehicle-treated (n = 4) and cilostazol-treated (n = 5) Tg-SwDI mice aged 15 months treated from 1.5 months. Error bars indicate SD. $^{*}P < 0.05$ in vehicle-treated Tg-SwDI mice versus cilostazol-treated Tg-SwDI mice.

cilostazol treatment helps to maintain efficient perivascular drainage of Aβ in Tg-SwDI mice.

Cilostazol reduced Aβ deposits in the Tg-SwDI mice brain

Tg-SwDI mice develop robust accumulation of both vascular and parenchymal Aβ deposits with predominance of $Aβ_{1-40}$ over $Aβ_{1-42}$ in the perivascular/vascular areas starting at 3 to 5 months of age (Fig. S7A–D).[37] We hypothesized that facilitation of perivascular Aβ drainage with cilostazol reduces Aβ deposits. Thus, we assessed the effects of cilostazol on Aβ accumulation in the Tg-SwDI mice brain. Cilostazol-treated Tg-SwDI mice showed significantly or marginally significantly decreased immunoreactivity of Aβ in the frontal cortex (Fig. 4A) and hippocampus (Fig. 4B) compared with vehicle-treated Tg-SwDI mice both aged 12 months (frontal cortex, $P = 0.0495$; hippocampus, $P = 0.0495$) (Fig. 4C) and 15 months (frontal cortex, $P = 0.057$; hippocampus, $P = 0.029$) (Fig. 4D). Both vehicle- and cilostazol-treated Tg-SwDI mice did not show apparent microhemorrhage aged 15 months (Fig. S7E and F). The evaluation of the blood brain barrier (BBB) integrity using Evans blue also showed that the Tg-SwDI mouse aged 10 months did not exhibit apparent Evans blue extravasation into the central nervous system (CNS) parenchyma; however, Evans blue did diffuse throughout the extracellular space in non-neural tissue (e.g., kidney, heart, and liver) (Fig. S8). Taken together, the above results indicated that cilostazol

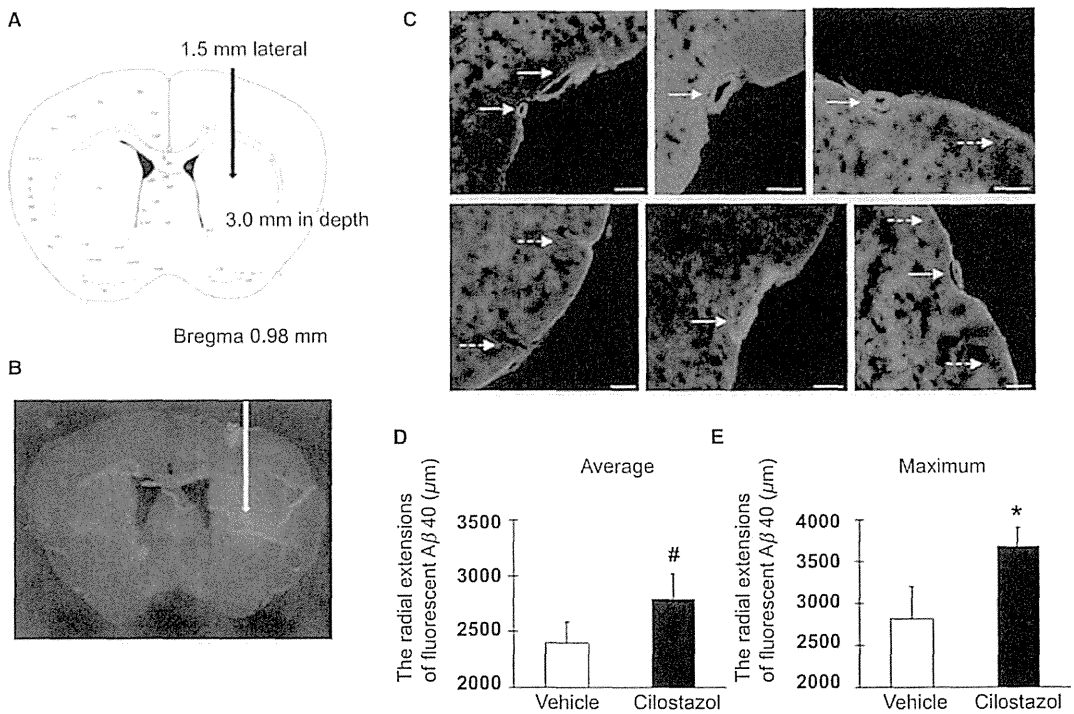

Figure 3. Facilitation of perivascular drainage of Aβ in cilostazol-treated Tg-SwDI mice. (A and B) A scheme (A) and coronal image (B) showing the site of the soluble fluorescent $A\beta_{1\text{-}40}$ injection (striatum; 0.98 mm anterior and 1.5 mm lateral from bregma, 3.0 mm in depth from the dorsal surface of the brain). (C) Representative double immunofluorescence images for laminin (red)/fluorescent $A\beta_{1\text{-}40}$ (green) in the leptomeningeal vessels 30 min after the injection of fluorescent $A\beta_{1\text{-}40}$ into the striatum. Solid arrow and dashed arrow indicate $A\beta_{1\text{-}40}$-positive and $A\beta_{1\text{-}40}$-negative staining, respectively. Scale bars indicate 100 μm. (D and E) Histograms showing the averaged (D) and maximal (E) values of radial extensions of fluorescent $A\beta_{1\text{-}40}$ in the leptomeningeal vessels from the site of injection (n = 3–4 for each group). Error bars indicate SD. *P < 0.05 and #P < 0.1 in vehicle-treated Tg-SwDI mice versus cilostazol-treated Tg-SwDI mice.

reduces Aβ accumulation in the Tg-SwDI mice brain possibly by promoting perivascular drainage of Aβ associated with preserved hemodynamic reserve.

Cilostazol attenuated the degradation of vascular walls with Aβ deposit

To examine the nature of Aβ accumulation and morphological changes in detail, we performed electron microscopy of Tg-SwDI mice aged 21 months that had been treated with cilostazol or vehicle for 17 months. Whereas 25% (49 per 195) of the vessels in the vehicle-treated Tg-SwDI mice showed some type of abnormality in the vascular wall vis-a-vis degeneration of pericytes or vascular smooth muscle cells or damaged intracellular organelles and alterations in the basement membranes (Fig. 5A–C, and Fig. S9A–D), only 6.4% (10 vessels per 155) of the vessels was affected in the cilostazol-treated mice (Fig. 5D–F, and Fig. S9E and F). The majority of degenerating pericytes in vehicle-treated Tg-SwDI mice exhibited morphological changes related to severe cell injury. These were apparent as numerous large vesicles, membranes around portions of the cytoplasm (called isolation membrane), mitochondrial injury, lysosomal inclusions, and large lysosomes were found in the cytoplasm of pericytes, mostly markers of autophagy (Fig. 5A, and Fig. S9A and B). The arterioles of vehicle-treated Tg-SwDI mice showed a similar degeneration of vascular smooth muscle cells with vacuolization and destroyed organelles accompanied by basement membrane thickening/alterations (Fig. 5B, C, and Fig. S9C, D). Conversely, cilostazol-treated Tg-SwDI mice only rarely showed the above-abnormal findings (Fig. 5D–F, and Fig. S9E and F).

Cilostazol prevented the decline of cognitive and grooming performance in Tg-SwDI mice

To evaluate cognitive function, we examined behavioral performance by using the Y maze test. Alternations of entries in the arms of the Y maze were significantly increased in cilostazol-treated Tg-SwDI mice (67.0 ± 2.9%)

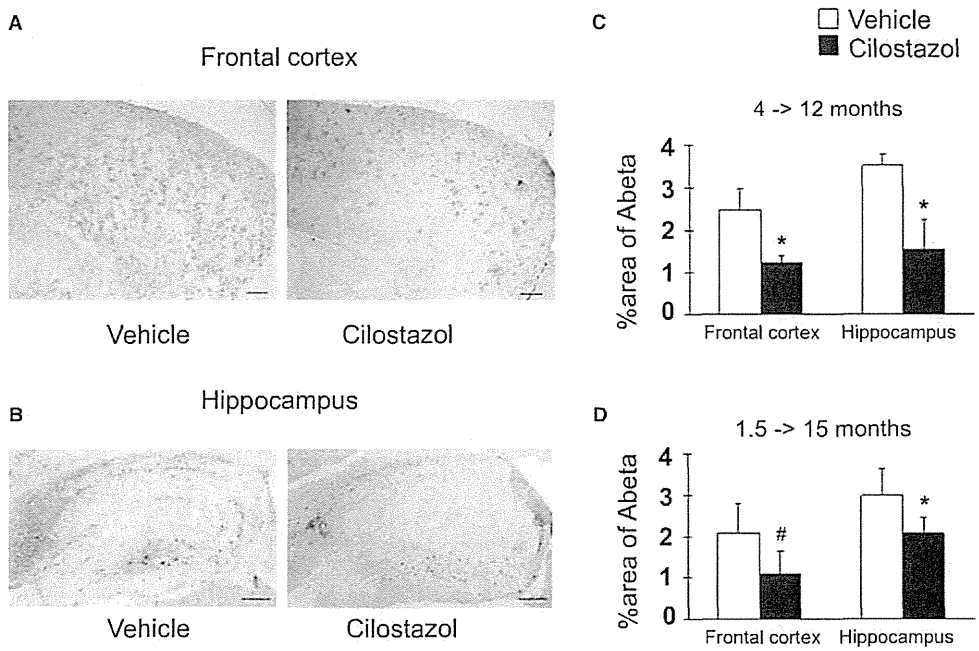

Figure 4. Cilostazol-treated Tg-SwDI mice exhibit reduced levels of Aβ deposits compared with vehicle-treated Tg-SwDI mice. (A and B) Representative images of Aβ staining in the frontal cortex (A) and hippocampus (B) in Tg-SwDI mice treated with vehicle (left) or cilostazol (right). Scale bars indicate 400 μm in A and 200 μm in B. (C and D) Histogram showing the density of cells immunoreactive for Aβ in the frontal cortex (left) and hippocampus (right) of vehicle-treated and cilostazol-treated Tg-SwDI mice aged 12 months treated from 4 months (C) and aged 15 months treated from 1.5 months (D) (n = 3–5 for each group). Values are expressed as mean ± SD. *P < 0.05 and #P < 0.1 in vehicle-treated Tg-SwDI mice versus cilostazol-treated Tg-SwDI mice.

compared with vehicle-treated mice (54.9 ± 3.3%) aged 12 months (P < 0.001; Fig. 6A, right panel). Spontaneous activity was not significantly different between the two groups of mice (Fig. 6A, left panel). At 15 months of age, although there was a trend for increase in alternations of entries in cilostazol-treated mice, no significant difference in both alternations of entries in the arms and spontaneous activity between vehicle- and cilostazol-treated Tg-SwDI mice (Fig. 6B). There were no significant differences in the number of total entries and alternations of entries between vehicle- and cilostazol-treated wild type mice aged 12 months (Fig. S10). Cilostazol-treated Tg-SwDI mice showed significantly better hair condition compared with vehicle-treated Tg-SwDI mice aged 15 months, also suggesting that cilostazol prevents cognitive decline in Tg-SwDI mice (Data S1 and Fig. S11).

Cilostazol suppressed endogenous Aβ production in the primary cultured neurons

There is a possibility that the observed reduction in Aβ deposition is a consequence of decreased Aβ production, in addition to increased Aβ clearance. Indeed, a previous study showed that cilostazol decreased extracellular and intracellular Aβ levels in mouse neuroblastoma N2a cells expressing human APP with Swedish mutation.[25] We examined the effect of cilostazol on endogenous Aβ production from neurons in vitro using the primary cultured rat neurons. This showed that cilostazol decreased the amount of Aβ40 and Aβ42 in the media released from neurons in a dose-dependent manner (Fig. 7A and B). A WST assay showed no significant differences among these groups (Fig. 7C). These results suggest that cilostazol can suppress the endogenous Aβ production from neurons without affecting cell viability.

Cilostazol did not affect APP processing in Tg-SwDI mice

Although cilostazol does reduce neuronal Aβ production, it has been established that only a very minor fraction of cilostazol can cross BBB and enter the brain after the peroral administration.[40] Therefore, the direct effects of cilostazol on neurons were expected to be less significant in vivo than in vitro. Based on the knowledge that β-secretase activity is augmented by hypoperfusion,[41] which may be ameliorated with cilostazol administration, we performed quantitative immunoblotting using antibody

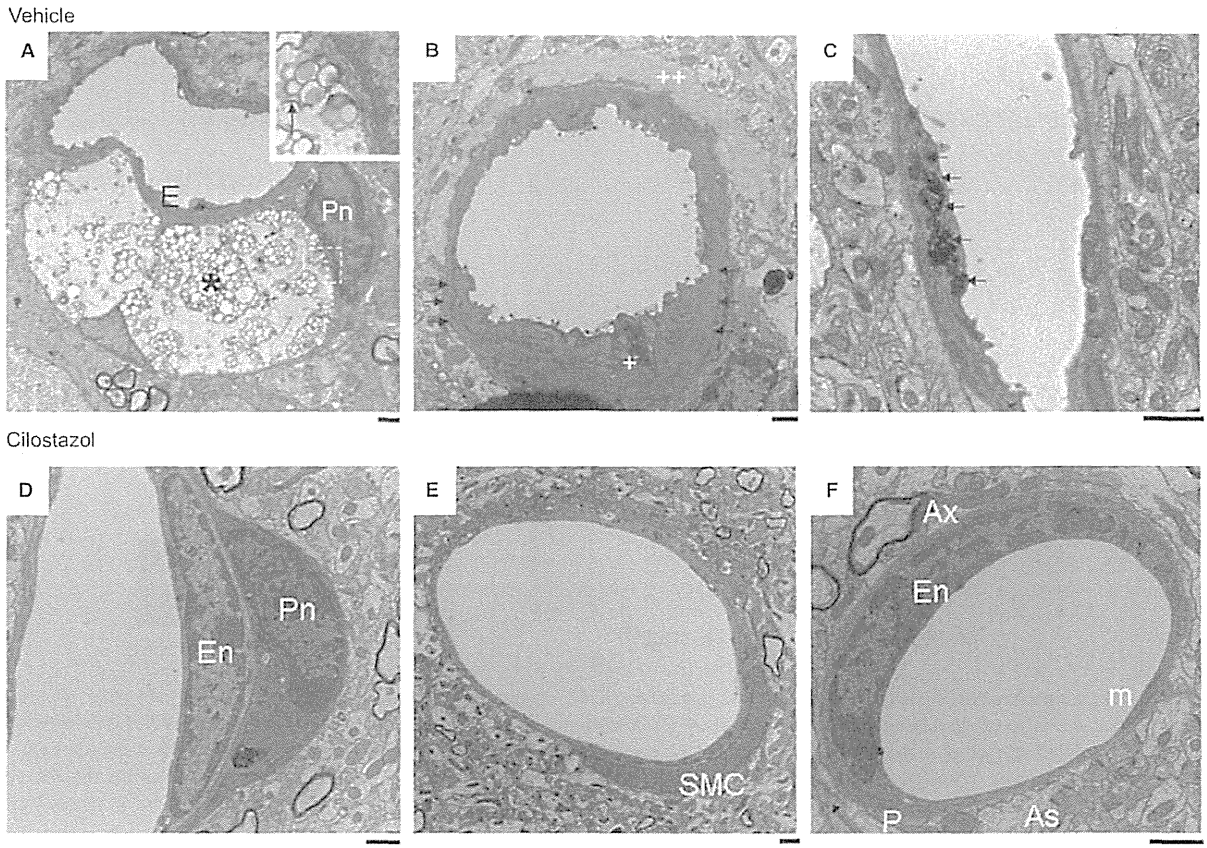

Figure 5. Electron microscopic images of vehicle-treated (A–C) and cilostazol-treated (D–F) Tg-SwDI mouse aged 21 months. The vehicle-treated Tg-SwDI mice showed marked degenerative changes of cerebral vessels, which were suppressed by long-term cilostazol treatment. (A) Numerous large vesicles and empty space were present in the cytoplasm of pericytes (*). *Inset*: Higher magnification of multiple vesicles (dashed square). The arrow indicates isolation membrane. (B) Degenerative changes of smooth muscle cells (+) accompanied with thickening/alterations of basement membrane (arrows) and amyloid fibril deposit (++). (C) Endothelial degeneration indicated by damaged intracellular organelles, replaced by dark materials (arrows). (D) Mild degenerative changes of pericyte were seen. Small vacuoles and dark materials in the cytoplasm of pericyte were present. (E) Almost intact arteriole. (F) Almost intact capillary. Scale bars indicate 1 μm. As, astrocyte; Ax, axon; BM, basement membrane; E, endothelial cell; En, nucleus of endothelial cell; m, mitochondrion; P, pericyte; Pn, nucleus of pericyte; SMC, smooth muscle cell.

against APP C-terminal domain, as a marker of APP processing. There were no significant differences in the levels of APP and APP C-terminal fragments (CTFs) between vehicle- and cilostazol-treated Tg-SwDI mice aged 15 months, which had received vehicle or cilostazol for 13.5 months (Fig. 8).

Discussion

The complex expression patterns and activity of the different PDEs throughout the CNS under normal and pathological conditions have been the subject of intense interest during the past decade, especially in regard to the therapeutic potential of PDE inhibitors for CNS disorders.[22,23] We found that PDE IIIA expression in the microvessels, predominantly in the smooth muscle cell layers, was markedly upregulated as CAA severity increased. To our knowledge, this is a first report showing the upregulation of PDE IIIA expression in the microvessels in close correlation with vascular amyloid burden. Further studies, including in vitro studies, are needed to clarify whether the increased PDE IIIA expression is a cause or consequence of amyloid deposit.

Our experimental study demonstrated that cilostazol, PDE III inhibitor, restores vascular reactivity and hemodynamic reserve, promotes perivascular drainage of Aβ, reduces degenerative changes of vascular walls with Aβ deposits and prevents the decline of cognitive performance in the Tg-SwDI mice, a model for cerebrovascular β-amyloidosis. These protective roles of cilostazol against Aβ-induced neurodegeneration seem to be mediated by its vasculotropic, but not antiplatelet, effects, as long-term

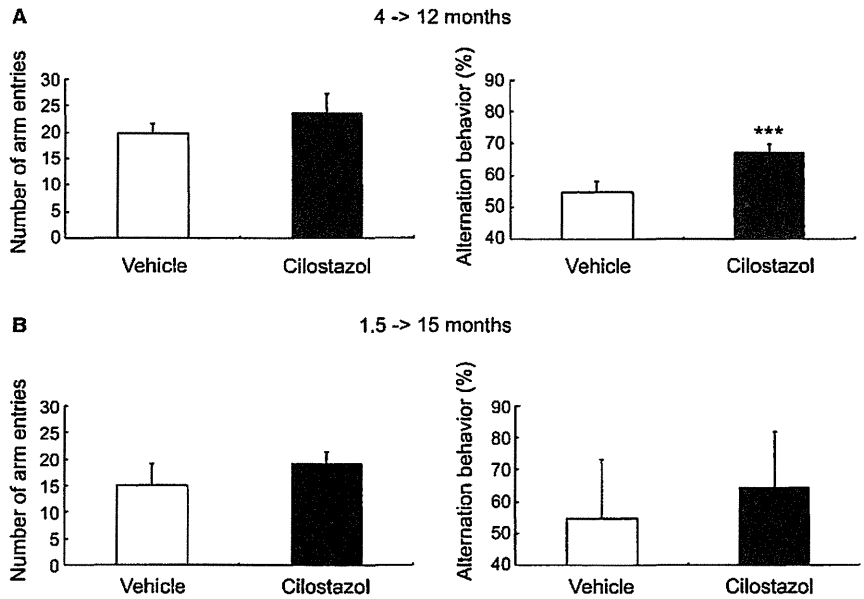

Figure 6. Cilostazol prevents working memory deficits in Tg-SwDI mice. (A) Histograms showing a number of arm entries (left) and alternation behavior (right) in the Y maze test of vehicle-treated (n = 11) and cilostazol-treated (n = 11) Tg-SwDI mice aged 12 months treated from 4 months. (B) Histograms showing number of arm entries (left) and alternation behavior (right) in the Y maze test of vehicle-treated (n = 10) and cilostazol-treated (n = 10) Tg-SwDI mice aged 15 months treated from 1.5 months. Error bars indicate SD. ***P < 0.001 in vehicle-treated Tg-SwDI mice versus cilostazol-treated Tg-SwDI mice.

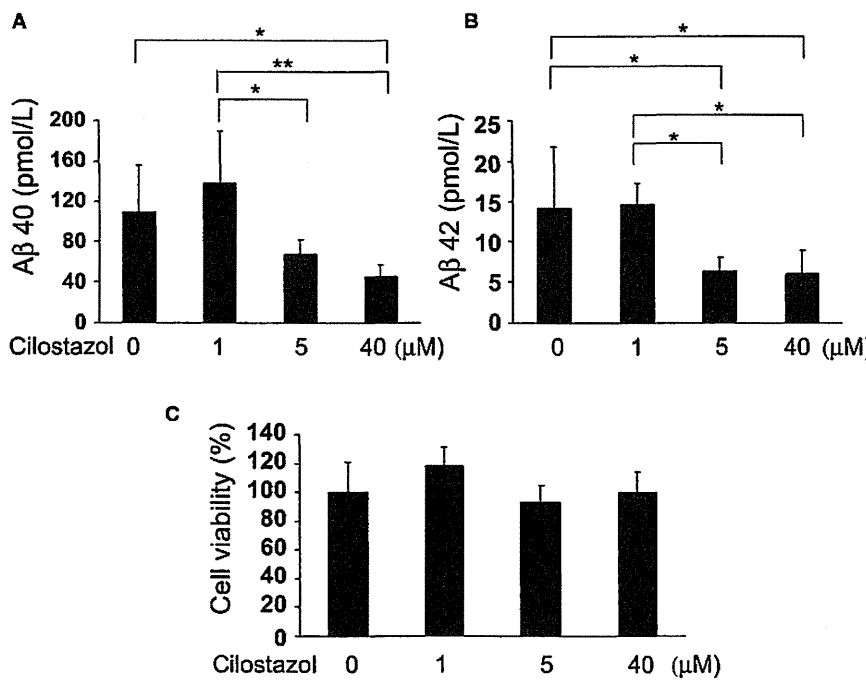

Figure 7. Cilostazol suppresses endogenous Aβ40 and Aβ42 production from cultured neurons. (A and B) The concentrations of Aβ40 (A) and Aβ42 (B) in the conditioned media from cultured rat neurons were measured by ELISA at 48 h after treatment with different concentration of cilostazol (1–40 μM). (C) WST assay using samples from cultured rat neurons at 48 h after treatment with different concentration of cilostazol (1–40 μM). N = 6 each. Values are mean ± SD. *P < 0.05, * *P < 0.01.

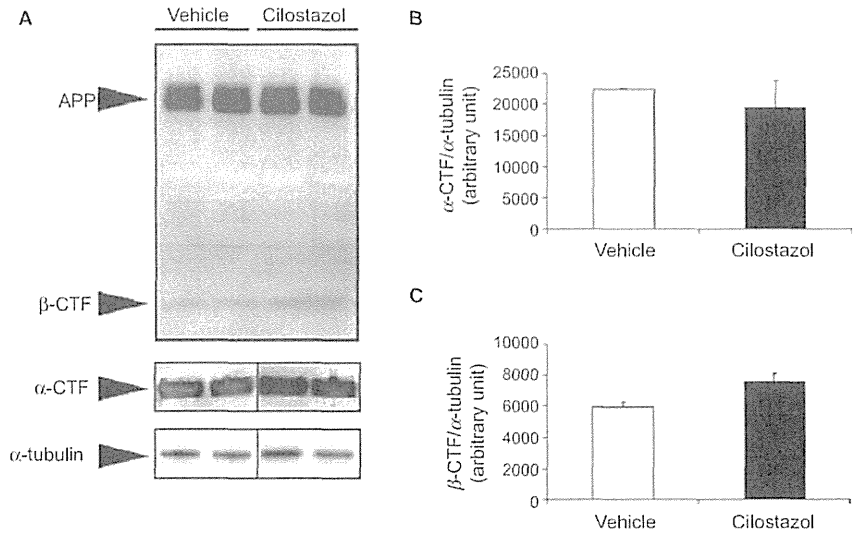

Figure 8. Cilostazol does not alter amyloid precursor protein (APP) processing in Tg-SwDI mice. (A) Western blot images of full length APP, APP C-terminal fragments (CTFs), β-CTF and α-CTF, and α-tubulin using protein extracts from the brain tissue of vehicle- and cilostazol-treated Tg-SwDI mice (n = 2–3 for each group) aged 15 months receiving vehicle or cilostazol for 13.5 months. For full-length APP, β-CTF, and α-tubulin, 50 μg protein lysates were applied in each well while 5 μg of protein lysates were applied to circumvent "white bands" for α-CTF. (B and C) Semiquantitative analysis of α-CTF (B) and β-CTF (C) normalized for α-tubulin. Values are mean ± SD.

aspirin treatment did not reverse vascular Aβ deposition, hemodynamic derangements, or cognitive decline in Tg-SwDI mice (unpublished data). Thus, besides its antiplatelet actions, the maintenance of neurovascular integrity with cilostazol could represent a promising approach in the decelerating cognitive decline associated with Aβ deposition. Since the motive force for perivascular Aβ drainage appears to be generated by arterial pulsations,[42,43] the direct action of cilostazol on the vascular smooth muscle cells to increase pulse duration time[32] and arterial elasticity[33] may have contributed to the facilitated perivascular drainage of Aβ and the above positive effects of cilostazol in the Tg-SwDI mice. Furthermore, as electron microscopic examinations have revealed, the protection of pericytes and other vascular components by cilostazol may have led to the preservation of vasodilative and hemodynamic reactivity and BBB integrity along the perivascular drainage pathway.

The CNS is devoid of conventional lymphatic vessels, unlike other organs that contain networks of lymphatic vessels, which process various elements such as wastes, fluid, proteins, and cells from tissues to lymph nodes.[15,42] However, the perivascular drainage system in the brain performs the main function assigned to systemic lymphatic vessels.[13–15,42,44] Animal studies using various tracers have demonstrated that interstitial fluid and solutes drain rapidly via perivascular "lymphatic" pathways from brain parenchyma along basement membranes in the walls of capillaries and arteries in the opposite direction of the arterial blood flow to cervical lymph nodes.[15,17,42] This drainage route corresponds very closely with the distribution of Aβ in the basement membranes of capillary and artery walls in CAA.[45] The failure of this drainage in the ageing brain and in the presence of CAA results in the accumulation of insoluble and soluble Aβ and probably other metabolites that would lead to loss of homeostasis of the neuronal environment.[15,42] This notion is also supported by the experimental data that the vascular Aβ deposition is increased following bilateral common carotid artery stenosis of CAA model mice[46] or middle cerebral artery occlusion model mice.[47] Such "lymphatic" congestion of the brain may be improved by vasoactive cilostazol.

Nevertheless, there is a possibility that the observed reduction in Aβ deposition could largely be a consequence of decreased Aβ production, rather than increased Aβ clearance. According to previous studies, cilostazol could regulate APP processing via the cAMP-PKA pathway or activation of CREB cascade,[26] and PKA has been implicated in the regulation of APP processing.[48] In addition, the PDE V inhibitor sildenafil has been shown to reduce brain Aβ through the cGMP-CREB pathway.[49] Given that the activation of the 5-HT4 receptor could regulate α-secretase activity, which is associated with cAMP functional response,[50] cilostazol-mediated cAMP might enhance α-secretase activity, leading to decreased Aβ production. Indeed, the current study showed that cilostazol could decrease endogenous Aβ generation from

the cultured neurons in vitro. There is also a possibility that the improvement of cerebral hemodynamics by cilostazol could reduce in Aβ synthesis as hypoxia/hypoperfusion has been shown to upregulate β-secretase BACE1.[41] However, cilostazol did not alter the levels of APP CTFs in Tg-SwDI mice in vivo. This discrepancy could be attributed to the poor ability of cilostazol to cross the BBB,[40] as well as the finding that BBB was not apparently disrupted in middle-aged Tg-SwDI mice in the current study. It is nonetheless possible that cilostazol, even at a low level, activates cAMP-PKA signaling with a similar mechanism to enriched environment, leading to the activation of β2-adrenergic receptors and inhibition of synaptotoxicity of human Aβ oligomers.[51] Taken together, the positive effects of cilostazol in vivo observed in the current study may predominantly result from facilitated Aβ clearance due to the sustained cerebrovascular function; however, the previously unidentified mechanisms leading to Aβ reduction, could offer a potential source of future investigation.

The use of Tg-SwDI mice has two distinctive advantages, when compared to other types of Tg mice harboring mutant APP. Firstly, Tg-SwDI mice have been shown to express mutant human APP at low levels, even below those of endogenous mouse APP in the brain. Despite the low expression levels of mutant APP, Tg-SwDI mice develop early-onset robust accumulation of Aβ in the brain. This could result from the deficient clearance of Dutch/Iowa mutant Aβ from the CNS at the cerebral vasculature, as shown in the previous studies.[37,52] Since decreased elimination, rather than increased production, of Aβ is likely to be a major cause of sporadic late-onset AD, this model would be useful for investigating the mechanisms and therapeutic approaches for sporadic AD. Second, Dutch/Iowa mutant Aβ peptides have highly vasculotropic nature and Tg-SwDI mice exhibit extensive microvascular amyloid deposition. A recent report showed that Tg-SwDI mice, which dominantly develop microvascular amyloid exhibit cognitive dysfunction at 3 months of age. However, Tg-5 × FAD mice that dominantly develop parenchymal amyloid deposits did not exhibit cognitive dysfunction at this age. These findings suggest that cerebral microvascular pathology might contribute to the early stages of cognitive impairment in AD and related disorders,[53] consistent with the notion that cerebral vascular dysfunction is an early contributor for AD pathophysiology.[2] The positive effects of cilostazol on Tg-SwDI mice in the current study suggest that cilostazol is a promising therapeutic target for early stages of cognitive impairment of neurodegenative etiology.

There are several issues to be addressed in future studies. First, we focused on only middle-aged and old Tg-SwDI mice, although emerging evidence shows that early vascular changes may precede Aβ accumulation and progressive disease cascades. Further studies are needed to elucidate whether cilostazol can improve early vascular alterations in young Tg-SwDI mice. Second, we specifically focused on perivascular drainage of Aβ. However, other clearance mechanisms, such as transcytotic delivery across BBB or degradation of Aβ by microglial/astroglial cells or enzymes, might contribute to reduction of Aβ overload. In addition, clearance pathways other than perivascular lymphatic routes, such as paravenous routes and bulk fluid flow through astrocytic endfeet[54] or paraaxonal/neuronal pathways, should be considered in future studies. Finally, the current study shows that cilostazol reduces Aβ overload by hemodynamic enhancement. However, the accumulation of NFTs within neurons, composed largely of ubiquitin and the microtubule-associated protein tau, is another important hallmark of AD.[1] While the accumulation of Aβ may derive mainly from the failure of the clearance system as mentioned above, that of NFTs appears to be associated at least partially with the failure of the ubiquitin-proteasome system.[16] Additionally, hemodynamic insufficiency has been shown to enhance phosphorylation of tau through upregulation of tau phosphorylating enzymes.[55] Further studies are warranted to examine whether cilostazol have positive effects on the neuropathology of NFTs as well as Aβ.

In conclusion, our study showed that the vasoactive drug cilostazol, a PDE III inhibitor, prevented cognitive decline triggered with Aβ deposition by facilitating Aβ clearance out of the brain and preserving neurovascular unit. Cilostazol, which can resolve the failure of the Aβ drainage pathway may provide a novel promising therapeutic target for AD/CAA, potentially in combination with early Aβ immunization therapy and pharmacological intervention to enhance enzymatic degradation of Aβ and absorption of Aβ into the blood. A prospective trial is now needed to determine the effects of cilostazol on AD/CAA.

Acknowledgment

We thank Professor Hidefumi Ito and Professor Roy Weller for their insightful discussions, as well as Dr. Akira Kuzuya and Dr. Laibaik Park for their technical advice. We are indebted to Tadanori Yamaguchi and Takako Kawada for their excellent technical assistance and Ahmad Khundakar for his editorial assistance and comments. We gratefully acknowledge grant support from the Ministry of Health, Labour and Welfare (M. I., No. 0605-1), the Ministry of Education, Culture, Sports, Science and Technology (M. I., Scientific Research (B), No. 23390233), the Takeda Science Foundation (M. I.), the National Institutes of Health (K. A., E. H. L., P01 NS055104; K. A.,

R01 NS065089; E. H. L., R37 NS037074), the Research Councils UK and Alzheimer's Research UK (R. N. K.), the Japan Society for the Promotion of Science (T. M.), and the Uehara Memorial Foundation (T. M.).

Author Contribution

T. M., designed the study, performed the experiments, analyzed and interpreted the data and wrote the manuscript; Y. O., Y. H., Y. H., S. S., Y. Y., Y. T., performed experiments, analyzed, and interpreted the data; R. O. C. and C. A. H.; interpreted the data, supervised and made critical revision of the manuscript for important intellectual content; H. I.-U., A. T, R. T, T. M., R. N. K., E. H. L., and K. A., supervised and made critical revision of the manuscript for important intellectual content; M. I., designed the entire study, handled funding, supervised all portions of the study, and wrote the manuscript.

Conflict of Interest

None declared.

References

1. Hardy J, Selkoe DJ. The amyloid hypothesis of Alzheimer's disease: progress and problems on the road to therapeutics. Science 2002;297:353–356.
2. Iadecola C. Neurovascular regulation in the normal brain and in Alzheimer's disease. Nat Rev Neurosci 2004;5:347–360.
3. Kalaria RN, Akinyemi R, Ihara M. Does vascular pathology contribute to Alzheimer changes? J Neurol Sci 2012;322:141–147.
4. Zlokovic BV. Neurovascular pathways to neurodegeneration in Alzheimer's disease and other disorders. Nat Rev Neurosci 2011;12:723–738.
5. Park L, Wang G, Zhou P, et al. Scavenger receptor CD36 is essential for the cerebrovascular oxidative stress and neurovascular dysfunction induced by amyloid-beta. Proc Natl Acad Sci USA 2011;108:5063–5068.
6. Miyakawa T. Vascular pathology in Alzheimer's disease. Psychogeriatrics 2010;10:39–44.
7. Mawuenyega KG, Sigurdson W, Ovod V, et al. Decreased clearance of CNS beta-amyloid in Alzheimer's disease. Science 2010;330:1774.
8. Wyss-Coray T, Loike JD, Brionne TC, et al. Adult mouse astrocytes degrade amyloid-beta in vitro and in situ. Nat Med 2003;9:453–457.
9. Hickman SE, Allison EK, El Khoury J. Microglial dysfunction and defective beta-amyloid clearance pathways in aging Alzheimer's disease mice. J Neurosci 2008;28:8354–8360.
10. Iwata N, Tsubuki S, Takaki Y, et al. Identification of the major Abeta1-42-degrading catabolic pathway in brain parenchyma: suppression leads to biochemical and pathological deposition. Nat Med 2000;6:143–150.
11. Deane R, Du Yan S, Submamaryan RK, et al. RAGE mediates amyloid-beta peptide transport across the blood-brain barrier and accumulation in brain. Nat Med 2003;9:907–913.
12. Sagare A, Deane R, Bell RD, et al. Clearance of amyloid-beta by circulating lipoprotein receptors. Nat Med 2007;13:1029–1031.
13. Hawkes CA, Sullivan PM, Hands S, et al. Disruption of arterial perivascular drainage of amyloid-beta from the brains of mice expressing the human APOE epsilon4 allele. PLoS One 2012;7:e41636.
14. Hawkes CA, Hartig W, Kacza J, et al. Perivascular drainage of solutes is impaired in the ageing mouse brain and in the presence of cerebral amyloid angiopathy. Acta Neuropathol 2011;121:431–443.
15. Weller RO, Preston SD, Subash M, Carare RO. Cerebral amyloid angiopathy in the aetiology and immunotherapy of Alzheimer disease. Alzheimers Res Ther 2009;1:6.
16. Weller RO, Boche D, Nicoll JA. Microvasculature changes and cerebral amyloid angiopathy in Alzheimer's disease and their potential impact on therapy. Acta Neuropathol 2009;118:87–102.
17. Arbel-Ornath M, Hudry E, Eikermann-Haerter K, et al. Interstitial fluid drainage is impaired in ischemic stroke and Alzheimer's disease mouse models. Acta Neuropathol 2013;126:353–364.
18. Sperling R, Salloway S, Brooks DJ, et al. Amyloid-related imaging abnormalities in patients with Alzheimer's disease treated with bapineuzumab: a retrospective analysis. Lancet Neurol 2012;11:241–249.
19. Smith EE, Schneider JA, Wardlaw JM, Greenberg SM. Cerebral microinfarcts: the invisible lesions. Lancet Neurol 2012;11:272–282.
20. Patton RL, Kalback WM, Esh CL, et al. Amyloid-beta peptide remnants in AN-1792-immunized Alzheimer's disease patients: a biochemical analysis. Am J Pathol 2006;169:1048–1063.
21. Boche D, Zotova E, Weller RO, et al. Consequence of Abeta immunization on the vasculature of human Alzheimer's disease brain. Brain 2008;131:3299–3310.
22. Garcia-Osta A, Cuadrado-Tejedor M, Garcia-Barroso C, et al. Phosphodiesterases as therapeutic targets for Alzheimer's disease. ACS Chem Neurosci 2012;3:832–844.
23. Menniti FS, Faraci WS, Schmidt CJ. Phosphodiesterases in the CNS: targets for drug development. Nat Rev Drug Discov 2006;5:660–670.
24. Hiramatsu M, Takiguchi O, Nishiyama A, Mori H. Cilostazol prevents amyloid beta peptide(25-35)-induced memory impairment and oxidative stress in mice. Br J Pharmacol 2010;161:1899–1912.
25. Park SH, Kim JH, Bae SS, et al. Protective effect of the phosphodiesterase III inhibitor cilostazol on amyloid

beta-induced cognitive deficits associated with decreased amyloid beta accumulation. Biochem Biophys Res Commun 2011;408:602–608.
26. Arai H, Takahashi T. A combination therapy of donepezil and cilostazol for patients with moderate Alzheimer disease: pilot follow-up study. Am J Geriatr Psychiatry 2009;17:353–354.
27. Sakurai H, Hanyu H, Sato T, et al. Effects of cilostazol on cognition and regional cerebral blood flow in patients with Alzheimer's disease and cerebrovascular disease: a pilot study. Geriatr Gerontol Int 2013;13:90–97.
28. Bell RD, Winkler EA, Singh I, et al. Apolipoprotein E controls cerebrovascular integrity via cyclophilin A. Nature 2012;485:512–516.
29. Bell RD, Winkler EA, Sagare AP, et al. Pericytes control key neurovascular functions and neuronal phenotype in the adult brain and during brain aging. Neuron 2010;68:409–427.
30. Chen WJ, Chen YH, Lin KH, et al. Cilostazol promotes vascular smooth muscles cell differentiation through the cAMP response element-binding protein-dependent pathway. Arterioscler Thromb Vasc Biol 2011;31:2106–2113.
31. Matsumoto S, Shimodozono M, Miyata R, Kawahira K. Effect of cilostazol administration on cerebral hemodynamics and rehabilitation outcomes in poststroke patients. Int J Neurosci 2011;121:271–278.
32. Aruna D, Naidu MU. Pharmacodynamic interaction studies of Ginkgo biloba with cilostazol and clopidogrel in healthy human subjects. Br J Clin Pharmacol 2007;63:333–338.
33. Han SW, Lee SS, Kim SH, et al. Effect of cilostazol in acute lacunar infarction based on pulsatility index of transcranial Doppler (ECLIPse): a multicenter, randomized, double-blind, placebo-controlled trial. Eur Neurol 2012;69:33–40.
34. Hase Y, Okamoto Y, Fujita Y, et al. Cilostazol, a phosphodiesterase inhibitor, prevents no-reflow and hemorrhage in mice with focal cerebral ischemia. Exp Neurol 2012;233:523–533.
35. Ihara M, Nishino M, Taguchi A, et al. Cilostazol add-on therapy in patients with mild dementia receiving donepezil: a retrospective study. PLoS One 2014;9:e89516.
36. Taguchi A, Takata Y, Ihara M, et al. Cilostazol improves cognitive function in patients with mild cognitive impairment: a retrospective analysis. Psychogeriatrics 2013;13:164–169.
37. Davis J, Xu F, Deane R, et al. Early-onset and robust cerebral microvascular accumulation of amyloid beta-protein in transgenic mice expressing low levels of a vasculotropic Dutch/Iowa mutant form of amyloid beta-protein precursor. J Biol Chem 2004;279:20296–20306.
38. Dumas A, Dierksen GA, Gurol ME, et al. Functional magnetic resonance imaging detection of vascular reactivity in cerebral amyloid angiopathy. Ann Neurol 2012;72:76–81.
39. Chow N, Bell RD, Deane R, et al. Serum response factor and myocardin mediate arterial hypercontractility and cerebral blood flow dysregulation in Alzheimer's phenotype. Proc Natl Acad Sci USA 2007;104:823–828.
40. Akiyama H, Kudo S, Shimizu T. The absorption, distribution and excretion of a new antithrombotic and vasodilating agent, cilostazol, in rat, rabbit, dog and man. Arzneimittelforschung 1985;35:1124–1132.
41. Sun X, He G, Qing H, et al. Hypoxia facilitates Alzheimer's disease pathogenesis by up-regulating BACE1 gene expression. Proc Natl Acad Sci USA 2006;103:18727–18732.
42. Weller RO, Djuanda E, Yow HY, Carare RO. Lymphatic drainage of the brain and the pathophysiology of neurological disease. Acta Neuropathol 2009;117:1–14.
43. Schley D, Carare-Nnadi R, Please CP, et al. Mechanisms to explain the reverse perivascular transport of solutes out of the brain. J Theor Biol 2006;238:962–974.
44. Carare RO, Bernardes-Silva M, Newman TA, et al. Solutes, but not cells, drain from the brain parenchyma along basement membranes of capillaries and arteries: significance for cerebral amyloid angiopathy and neuroimmunology. Neuropathol Appl Neurobiol 2008;34:131–144.
45. Revesz T, Ghiso J, Lashley T, et al. Cerebral amyloid angiopathies: a pathologic, biochemical, and genetic view. J Neuropathol Exp Neurol 2003;62:885–898.
46. Okamoto Y, Yamamoto T, Kalaria RN, et al. Cerebral hypoperfusion accelerates cerebral amyloid angiopathy and promotes cortical microinfarcts. Acta Neuropathol 2012;123:381–394.
47. Garcia-Alloza M, Gregory J, Kuchibhotla KV, et al. Cerebrovascular lesions induce transient beta-amyloid deposition. Brain 2011;134:3697–3707.
48. Xu H, Sweeney D, Greengard P, Gandy S. Metabolism of Alzheimer beta-amyloid precursor protein: regulation by protein kinase A in intact cells and in a cell-free system. Proc Natl Acad Sci USA 1996;93:4081–4084.
49. Puzzo D, Staniszewski A, Deng SX, et al. Phosphodiesterase 5 inhibition improves synaptic function, memory, and amyloid-beta load in an Alzheimer's disease mouse model. J Neurosci 2009;29:8075–8086.
50. Lezoualc'h F. 5-HT4 receptor and Alzheimer's disease: the amyloid connection. Exp Neurol 2007;205:325–329.
51. Li S, Jin M, Zhang D, et al. Environmental novelty activates beta2-adrenergic signaling to prevent the impairment of hippocampal LTP by Abeta oligomers. Neuron 2013;77:929–941.
52. Davis J, Xu F, Miao J, et al. Deficient cerebral clearance of vasculotropic mutant Dutch/Iowa Double A beta in

human A betaPP transgenic mice. Neurobiol Aging 2006;27:946–954.
53. Xu W, Xu F, Anderson ME, et al. Cerebral microvascular rather than parenchymal amyloid-beta protein pathology promotes early cognitive impairment in transgenic mice. J Alzheimers Dis 2014;38:621–632.
54. Iliff JJ, Wang M, Liao Y, et al. A paravascular pathway facilitates CSF flow through the brain parenchyma and the clearance of interstitial solutes, including amyloid beta. Sci Transl Med 2012;4:147ra111.
55. Koike MA, Green KN, Blurton-Jones M, Laferla FM. Oligemic hypoperfusion differentially affects tau and amyloid-{beta}. Am J Pathol 2010;177:300–310.

Supporting Information

Additional Supporting Information may be found in the online version of this article:

Data S1. Supplemental materials.
Data S1. Supplemental data.
Figure S1. The correlation between the CAA severity and the PDE IIIA expression score demonstrates significant linear correlation ($Rs = 0.8272$, $P < 0.001$). PDE IIIA expression score was calculated from the average of qualified grading of PDE IIIA expression (0 = none, 1 = low, 2 = medium, 3 = high).
Figure S2. (A–E) Representative images of PDE IIIA immunostaining in patients with AD and CAA. PDE IIIA expression is only slightly observed in neurites in the cerebral cortex (A) and pyramidal neurons in the hippocampal CA3 regions (B) and dentate gyrus (C), whereas it is strong in the cortical vessels in patients with AD/CAA (D, E). Scale bar indicates 50 μm.
Figure S3. Representative images of the leptomeningeal arteries (A–D), the cerebral cortex (E–H), and the senile plaques (I–L), which were stained for Aβ (A, E, I), paired helical filament-tau (PHF-tau) (B, F, J), PDE IIIA (C, G, K), and Congo red (D, H, L) in patients with AD and CAA. Of note, some neurons with dystrophic neurites (J, dashed arrow) showed PDE IIIA expression (G, K), but neuropil threads (F, arrows) and amyloid cores (I and L, arrows) were not positive for PDE IIIA. Scale bar indicates 50 μm.
Figure S4. PDE IIIA expression is increased in the vascular wall in aged Tg-SwDI mouse. Representative images of PDE IIIA immnostaining in the leptomeningeal (A–C) and intracortical (D–F) arteries of wild type mouse aged 12 months (A and D), Tg-SwDI mouse aged 4 months (B, E), and Tg-SwDI mouse aged 23 months (C and F). Scale bar indicates 20 μm.
Figure S5. Thioflavin-S staining in the Tg-SwDI mouse aged 23 months. Scale bars indicate 100 μm in A–F, 1 mm in G, and 500 μm in H and I.
Figure S6. Representative images of vehicle- (A) and cilostazol-treated (B) Tg-SwDI mice showing where vessel diameter was quantified. An averaged vessel diameter across a 25 μm longitudinal segment (8 consecutive segments per mouse) was analyzed before (baseline) and after inhalation of 5% CO_2 or treatment with acetylcholine. Scale bars indicate 50 μm.
Figure S7. Tg-SwDI mice exhibit robust accumulation of both vascular and parenchymal Aβ with predominance of Aβ40 over Aβ42 in the perivascular/vascular areas without apparent microhemorrhage or BBB leakage at 15 months of age. (A–D) Representative images of Aβ40 (A), Aβ42 (B), and Aβ (6E10) immunostaining (C and D), Perls-Stieda's iron staining (E), and IgG staining (F) in Tg-SwDI mice aged 15 months. Scale bars indicate 50 μm in A and B, 20 μm in C and D, and 100 μm in E and F.
Figure S8. Representative macroscopic (A and B) and microscopic fluorescent (C and D) images of the brain (A, C) and kidney (B and D) in the Tg-SwDI mouse aged 10 months after Evans blue, followed by FITC dextran (green), injection. There were clear differences in the extravascular extravasation of Evans blue (shown in blue in A, B, and red in C, D) between the brain and kidney. Scale bars indicate 50 μm.
Figure S9. Electron microscopic images of vehicle-treated (A–D) and cilostazol-treated (E, F) Tg-SwDI mice aged 21 months. (A) Multiple vesicles in the cytoplasm of pericytes. (B) Multiple vesicles (+) and damaged intracellular organelles including mitochondria replaced by dark material (upper inset) in the pericytic cytoplasm. Multiple vacuoles (++) and thickening/alterations of basement membrane (lower inset). The regions marked by dashed squares are enlarged in the right upper and lower inset, respectively. (C) Thickening/alterations of basement membrane. The region marked by a dashed square is enlarged in the inset. (D) Two transversely sectioned microvessels were seen connected by a dysmorphic process. Multiple stages of autosomes, lysosomes, and damaged intracellular organelles with disruption of mitochondrial membrane and reduced cristae (arrows, right lower inset) were present (++). The regions marked by dashed squares are enlarged in the right upper and lower inset, respectively. (E and F) Almost intact capillaries were seen in cilostazol-treated Tg-SwDI mice. Arrows indicate tight junction of endothelial cells. Pericytic mitochondria were normal. The region marked by a dashed square is enlarged (F, inset). Scale bars indicate 1 μm. As, astrocyte; Ax, axon; BM, basement membrane; E, endothelial cell; En, nucleus of endothelial cell; Ly, lysosome; m, mitochondrion; P,

pericyte; Pn, nucleus of pericyte.

Figure S10. (A) Histograms showing number of arm entries (left) and alternation behavior (right) in the Y maze test of vehicle-treated ($n = 10$) and cilostazol-treated ($n = 10$) wild type mice aged 12 months treated from 11 months of age. Error bars indicate SD.

Figure S11. Grooming performance in vehicle-treated and cilostazol-treated Tg-SwDI mice. (A) Images showing the hair (ruffled coat) conditions graded as four categories 0–3. (B) Histogram showing grading score of the hair (ruffled coat) condition of vehicle-treated ($n = 10$) and cilostazol-treated ($n = 12$) Tg-SwDI mice aged 15 months. Error bars indicate SEM. $^*P < 0.05$ in vehicle-treated Tg-SwDI mice versus cilostazol-treated Tg-SwDI mice.

Table S1. Detailed neuropathological features and analyses of 17 patients with AD or non-AD. These patients were also divided into 4 groups according to the Vonsattel grade of CAA (4 patients without CAA, 4 patients each with mild or moderate, and 5 patients with severe CAA). The grading score of PDE IIIA expression is calculated from the average of qualified grade (0 = none, 1 = low, 2 = medium, 3 = high). In total, 1700 leptomeningeal and cortical arteries (100 per patient) were analyzed in the randomly selected 5 regions (20 vessels per one region) from the temporal and occipital lobes. AD, Alzheimer's disease; ALS, amyotrophic lateral sclerosis; CAA, cerebral amyloid angiopathy; CERAD, Consortium to Establish a Registry for Alzheimer's Disease; CHF, congestive heart failure; CLL, Chronic lymphocytic leukemia; NFT, neurofibrillary tangle; SIVD, subcortical ischemic vascular dementia; VaD, vascular dementia; ND, not determined.

